Earthq Eng & Eng Vib (2019) 18: 871-886 **DOI**: https://doi.org/10.1007/s11803-019-0540-7

Experimental seismic behavior of squat shear walls with precast concrete hollow moulds

Han Wenlong[1, 2†], Zhao Zuozhou[1‡], Qian Jiaru[1‡], Zhang Yingbao[3§] and Ma Tao[4§]

1. *Key Laboratory of Civil Engineering Safety and Durability of China Education Ministry, Tsinghua University, Beijing 100084, China*
2. *China Institute of Building Standard Design & Research, Beijing 100048, China*
3. *Beijing Everest Green Building Technology Ltd., Beijing 102209, China*
4. *Beijing Institute of Architectural Design, Beijing 100045, China*

Abstract: This study proposes an innovative precast shear wall system, called an EVE precast hollow shear wall structure (EVE-PHSW). Precast panels in EVE-PHSW are simultaneously precast with vertical and horizontal holes. Noncontact lap splices of rebars are used in vertical joints connecting adjacent precast panels for automated prefabrication and easy in situ erection. The seismic behavior of EVE walls was examined through a series of tests on six wall specimens with aspect ratios of 1.0~1.3. Test results showed that EVE wall specimens with inside cast-in situ concrete achieved the desired "strong bending and weak shear" and failed in shear mode. Common main diagonal cracks and brittle shear failure in squat cast-in situ walls were prevented. Inside cast-in situ concrete could significantly improve the shear strength and stiffness of EVE walls. The details of boundary elements (cast-in situ or prefabricated) and vertical joints (contiguous or spaced) had little effect on the global behavior of EVE walls. Noncontact lap splices in vertical joints could enable EVE walls to exhibit stable load-carrying capacity through extensive deformations. Evaluation on design codes revealed that both JGJ 3-2010 and ACI 318-14 provide conservative estimation of shear strength of EVE walls, and EVE walls achieved shear strength reserves comparative to cast-in situ walls. The recommended effective stiffness for cast-in situ walls in ASCE 41-17 appeared to be appropriate for EVE walls.

Keywords: precast concrete hollow mould; low-aspect-ratio; noncontact lap splice; prefabricated boundary element; vertical and horizontal joints; seismic behavior

1 Introduction

Precast construction has achieved overwhelming success worldwide, especially in China over the last decade, due to better in situ control, accelerated construction and reduced in situ labor compared with conventional cast-in situ construction. Impacted by living habits and conventional cast-in situ concrete residential buildings, precast residential buildings in China are mostly designed as precast shear wall structures rather than precast frames, which are commonplace in the West and Japan but encounter great resistance in China. Precast shear wall structures can be classified into two categories according to the precast degree of the walls. The first category is the so-called fully precast wall structures which consist of precast full-thickness walls. Specialized rebar splices, such as grouted couplers (Peng *et al.*, 2015), are used to provide precast wall vertical rebars with continuity, resulting in high-cost connections and strict erection tolerance. The second consists of precast partial-thickness walls that function as outside formworks during in situ construction, namely superimposed shear wall structures. In these systems, superimposed walls are connected by cast-in situ concrete and additional spliced rebars, and no specialized rebar splice is needed. Hence, superimposed walls possess the merits of cast-in situ construction, achieving loose erection tolerance and accelerated construction. Superimposed wall structures are usually considered as equivalent monolithic systems, which are designed to closely emulate the seismic response of cast-in situ structures in terms of strength, stiffness, deformation and energy-dissipation characteristics. However, cast-in situ horizontal and vertical joints connecting adjacent precast walls significantly affect the abovementioned performance of superimposed wall structures.

More recently, superimposed walls with various precast panels and joints have been developed, such as the double wall system (Chong *et al.*, 2016 and 2017) and precast hollow mould system (Qian *et al.*, 2010; Zhou *et al.*, 2015; Chu *et al.*, 2017). Double walls consist

Correspondence to: Han Wenlong, China Institute of Building Standard Design & Research, Beijing 100048, China
Tel: +86-10-68799283; Fax: +86-10-68368656
E-mail: hanwenlong9122@163.com
†PhD, Engineer; ‡Professor; §Engineer
Received November 3, 2017; **Accepted** April 23, 2018

of two precast side panels connected by truss rebars. Tests on flexure-dominated double walls showed that they delivered global behavior comparative to their cast-in situ counterpart (Cai, 2015); vertical joints, which consist of concealed column, contiguous connection or spaced cast-in situ segment, can all satisfy the force transfer demand between adjacent precast panels (Wang *et al.*, 2012). However, reduced deformation and energy-dissipation capacities were observed in some tests, due to the concentrated gap opening at horizontal joints (Xiao and Guo, 2014; Chong *et al.*, 2016). To prevent this adverse gap opening, Chong *et al.* (2017) developed an enhanced horizontal joint for double walls using capacity-based design. Compared with double walls, precast panels in a precast hollow mould system are precast with inside holes, and the two outer wythes are connected by concrete ribs between inside holes rather than truss rebars. Qian *et al.* (2010) developed precast walls that consisted of precast panels with vertical circular holes and cast-in situ boundary elements (CBEs); however, inclined cracks on one precast panel could not continuously develop into the adjacent panel due to inadequate anchorage of horizontal rebars in vertical joints. To enhance the force transfer at vertical joints, Zhou *et al.* (2015) and Chu *et al.* (2017) developed precast hollow moulds with two-way (that is, horizontal and vertical) holes, in which wall horizontal distributed rebars were continuously placed in horizontal holes. Test results showed that flexure-dominated precast walls exhibited seismic behavior resembling their cast-in situ counterpart; however, shear strength of precast walls with vertical joints was about 20% lower than that of cast-in situ walls. In addition, it is difficult to insert horizontal rebars through the narrow horizontal holes in long walls; and the necessary CBEs for inserting horizontal rebars inevitably increase situ work and labor. These two attributions restrict the application of this two-way hollow mould system.

This study aims at developing an innovative precast two-way hollow mould system, called an EVE precast hollow shear wall structure (EVE-PHSW). To control cost and simplify in situ construction, noncontact lap splice (NLS) rather than specialized rebar splice is used at horizontal and vertical joints in the EVE-PHSW. The splice length l_d and clear transverse distance s between the two spliced rebars are key factors that affect the performance of NLS (Hamad and Mansour, 1996; Gilbert and Kilpatrick, 2015). For NLSs in cast-in situ structures, Sagan *et al.* (1988) proposed that NLS with $s \leq s_0$ (s_0 denotes the upper limit of s) could be conservatively designed as a contact lap splice in tension ignoring the effect of s, while the effect of s should be considered for NLS with $s > s_0$ through a recommended strut-and-tie model. However, various s_0 was recommended, for instance, 12d (d denotes the spliced rebar diameter) for monotonic and 8d for repeated inelastic loading in Sagan *et al.* (1988), while 4d in Eurocode 2 (2004) and CEB-FIP model code 1990 (1990). Compared with monolithic cast-in situ members, the precast to cast-in situ concrete interface in superimposed members may affect the performance of the NLSs. However, there have not been many studies of this phenomena.

An EVE-PHSW is developed from a critical review of the advantages and limitations of the abovementioned superimposed wall systems, which in turn are used or overcome. In this study, the concept of EVE-PHSW is developed and illustrated. Emphasis is given to the boundary elements and vertical joints connecting adjacent precast panels. In this regard, a series of quasi-static tests has been conducted on six EVE precast walls with aspect ratios (i.e., shear span-to-depth ratio) of 1.0–1.3. The test results (i) identify the feasibility of the joint details and NLSs, (ii) evaluate the seismic performance of squat EVE precast walls, and (iii) point out the advantages that this system can provide.

2 Concept of the proposed system

Figure 1 schematically shows the proposed EVE-PHSW, where standard precast panels are assembled together to achieve architectural plan layouts with different functions and sizes. At the intersection zone of walls in orthogonal directions, where plenty of rebars of orthogonal walls and boundary elements stagger, CBEs are used for easy construction and enhanced connections; at the side of windows or doors, prefabricated boundary elements (PBEs) are used to reduce in situ formwork and accelerate construction. NLSs provide vertical and horizontal rebars in precast panels with continuity. To accomplish this, precast panels are precast with vertical rounded rectangular holes and side horizontal rounded square holes. Vertical holes run through from bottom to top for pouring inside cast-in situ concrete, while horizontal holes are only placed at side concrete ribs for insertion of horizontal spliced rebars. Straight rebars and welded closed hoops are placed in vertical and horizontal holes as additional spliced rebars of vertical and horizontal joints, respectively. After pouring cast-in situ concrete, adjacent precast panels and CBEs are connected together by cast-in situ horizontal and vertical joints. The inside concrete ribs of precast panels connect the two outer wythes, and enhance the connection between the outer wythes and inside cast-in situ concrete. Shear keys form at horizontal and vertical holes and enhance the shear-resistance at these joints.

Compared with existing superimposed wall systems, the following advantages are achieved in EVE-PHSW. First, standard precast panels rather than various large panels are used, making it possible to produce panels efficiently by an automated production line. Second, PBEs are used at the sides of windows or doors, while CBEs are only used at intersection zones of walls in orthogonal directions, contributing to reduced in situ formwork and reinforcement assembly. Third, the use of NLSs in vertical joints avoids protruding horizontal

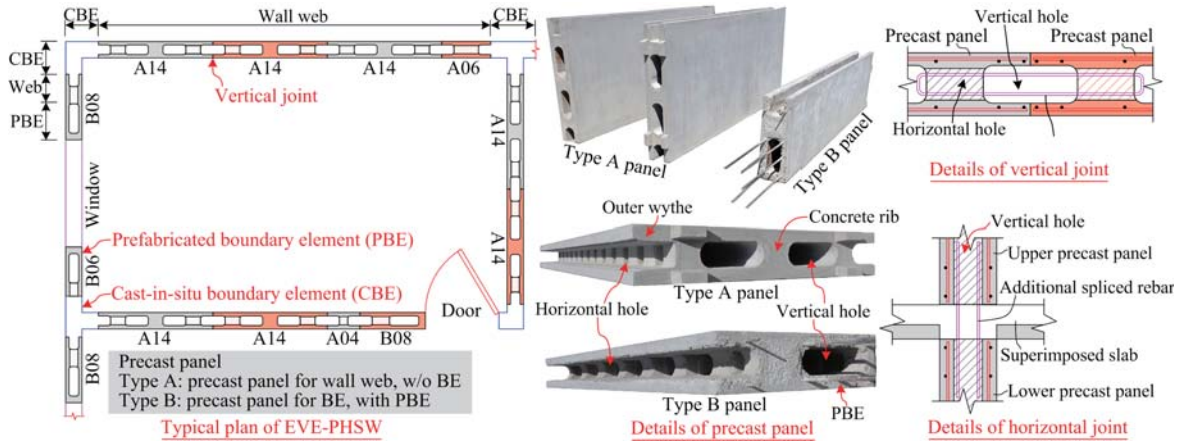

Fig. 1 Proposed EVE-PHSW

rebars and inserting horizontal rebars through narrow horizontal holes in long walls, contributing to easy in situ erection. Fourth, horizontal and vertical rebars in precast panels can be designed for shear and moment resistance due to the continuity provided by NLSs, reducing the reinforcement amount. Finally, NLSs, rather than specialized rebar splices, are used in both horizontal and vertical joints, resulting in loose erection tolerance and less protruding spliced rebars, which additionally improve the efficiency of automated product lines. All these enable EVE-PHSW to be a fast and low-cost construction system.

3 Experiment program

3.1 Specimen design

This study focuses on the shear behavior and vertical joint performance of EVE precast walls. Note that vertical joints in walls with shear failure mode suffer more critical stress states than those in walls with flexural failure mode; hence, specimens were designed with aspect ratios of 1.0–1.3 to ensure the shear-dominated deformation mode. A total of six specimens, labeled CS1.2, CS1.2H, CD1.3, PD1.3, PD1.3S and PT1.0, were designed and tested. Figure 2 illustrates the design details of specimens and Table 1 shows the test matrix. Each specimen consisted of a shear wall, a foundation beam and a loading beam. The foundation beam and loading beam were designed to remain in the elastic range as capacity-protected members. The walls of all specimens were 1920 mm tall to accommodate the loading facility, and had rectangular cross-sections with identical thickness t_w of 200 mm and different depth h_w. Three variables were considered in the wall design: (i) the type of boundary element, that is, CBE or PBE; (ii) details of vertical joints; and (iii) configuration of precast panels. These variables can be identified from the specimen labels, in which the first letter C or P denotes CBE or PBE, respectively; the second letter S, D, or T indicates that the specimen was assembled by one, two, or three precast panels to simulate configuration of precast panels in Fig. 1, respectively; figure 1.0, 1.2, or 1.3 denotes the aspect ratio of the specimen; and the last letter H indicates that the two middle vertical holes of the precast panel kept hollow without cast-in situ concrete, while the last letter S denotes the spaced vertical joint (SVJ). Specimens were divided into three groups. The first group consisted of Specimens CS1.2 and CS1.2H,

Table 1 Parameters of specimens

Specimen	h_w (mm)	Configuration	Parameter of NLS		Concrete strength $f_{cu,m}$ (MPa)			Axial load N (kN)
			l_d	s	Precast panel	Cast-in situ	Avg	
CS1.2	1800	CBE+A14+CBE	$40d$ ($1.0l_{aE}$)	$4.5d$	29.4	34.3	31.9	515
CS1.2H	1800	CBE+A14+CBE	$40d$ ($1.0l_{aE}$)	$4.5d$	29.4	33.8	26.2	515
CD1.3	1600	CBE+A06+A06+CBE	$42d$ ($1.05l_{aE}$)	$4.5d$	29.4	30.0	29.7	460
PD1.3	1600	B08+B08	$48d$ ($1.2l_{aE}$)	$6.0d$	29.4	30.0	29.6	460
PD1.3S	1600	B06+SVJ+B08	$40d$ ($1.0l_{aE}$)	$6.0d$	29.4	33.8	31.4	460
PT1.0	2000	B08+A04+B08	$40d$ ($1.0l_{aE}$)	$6.0d$	29.4	33.8	31.1	570

Note: A14, A06 and A04 denotes Type A precast panel with a width of 1400 mm, 600 mm and 400 mm, respectively; B08 and B06 denotes Type B precast panel with a width of 800 mm and 600 mm, respectively.

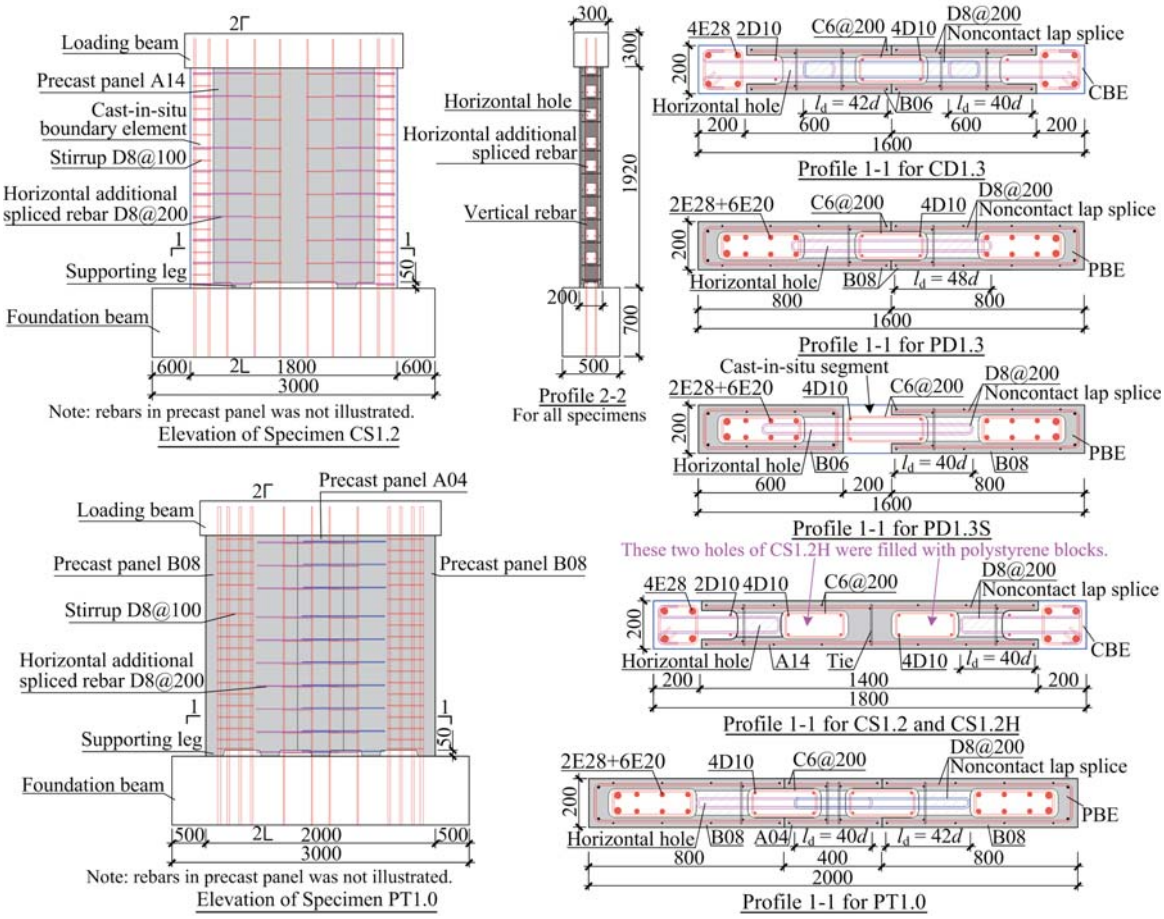

Fig. 2 Design details of specimens (unit: mm)

which had identical section properties. However, the two middle vertical holes in CS1.2H were filled with polystyrene blocks instead of concrete, while the upper and lower 250 mm high zones were filled with cast-in situ concrete to enhance slip-resistance. The effect of the inside cast-in situ concrete was studied through CS1.2 and CS1.2H. The second group consisted of Specimens CD1.3, PD1.3 and PD1.3S, which all were assembled by two precast panels and had identical h_w. The two precast panels of CD1.3 or PD1.3 were assembled in close contact and connected by contiguous vertical joints (CVJ); while precast panels of PD1.3S were spaced from each other by a 200 mm wide cast-in situ segment, and were connected by the SVJ. The performance of CBE and PBE was studied through CD1.3 and PD1.3, while the performance of CVJ and SVJ was identified through PD1.3 and PD1.3S. The third group included Specimen PT1.0, which consisted of three precast panels. Two CVJs formed in PT1.0, and the performance of EVE walls assembled by multiple precast panels was evaluated.

The concrete used for precast panels and cast-in situ concrete had a strength grade of C30 (nominal cubic compressive strength $f_{cu,d}$ = 30 MPa). Except for adopting low aspect ratios, all specimens were designed as "strong bending and weak shear" using capacity-based design. That is, the flexural strength of the specimen was significantly larger than the shear strength. To accomplish this, boundary elements were reinforced with large-diameter and high-strength HRB500 (nominal yield strength f_{yn} = 500 MPa) longitudinal reinforcement, while normal-strength HRB400 (f_{yn} = 400 MPa) rebars were used as horizontal rebars. Details of vertical joints in all specimens were identical to those used in actucal projects (Fig. 1), in which horizontal additional spliced rebars (HASR) overlap with horizontal distributed rebars of precast panels (HDRP) at the same height. Limited by the construction space, l_d and s of horizontal NLSs in different specimens were very similar. Table 1 summarizes l_d and s of each specimen, where l_{aE} denotes the seismic anchorage length of rebars in tension specified in GB 50010-2010 (2010). l_d of all specimens ranged from 40d (1.0l_{aE}) to 48d (1.2l_{aE}), which was significantly smaller than the required length for contact lap splices in tension, with all rebars lapped in the same section in GB 50010-2010 (= 1.6l_{aE}). Meanwhile, s of all specimens was 4.5d or 6.0d, consistent with the requirement in ACI 318-14 (2014) that s shall be at least the greatest of 1 in. (25.4 mm), d, and (4/3)d_{agg} (d_{agg} denotes nominal maximum size of coarse aggregate), and the transverse center-to-center spacing of spliced rebars shall not exceed the lesser of 152 mm and 0.2l_d.

3.2 Fabrication of specimens

All specimens were constructed in accordance with actual construction procedures. Precast panels were precast first by an automated product line; meanwhile, the lower foundation beams were constructed with wall longitudinal rebars projecting from the top. After assembling these pieces together, additional spliced rebars and rebars of boundary element were assembled. Finally, the loading beams were cast together with the lower wall by pouring cast-in situ concrete. Considering the specialized precast production technique and the narrow situ construction space, fine aggregate concrete with coarse aggregate maximum size of 10 mm, resembling that in actual projects, was used for precast panels and cast-in situ concrete to guarantee the concrete density. In addition, the top surface of the foundation beams in contact with the upper walls was rough surface; precast panels were equipped with 50 mm high supporting legs at the bottom (Fig. 2); after pouring the cast-in situ concrete, shear keys formed at horizontal joints, enhancing the slip resistance of these joints.

3.3 Material properties

Actual cubic compressive strength $f_{cu,m}$ of concrete was tested on cubes of 150 mm size, and the results are shown in Table 1. In Table 1, the average concrete cubic compressive strength of each specimen was calculated based on the area ratio of precast panels or cast-in situ concrete to the total wall cross-section. The test axial compressive strength of concrete $f_{c,m}$ was taken as $0.76f_{cu,m}$ according to GB 50010-2010.

The properties of rebars measured in tension tests are summarized in Table 2, where $f_{y,m}$,$f_{u,m}$, A_{gt}, ε_y denotes the measured yield strength, measured tensile strength, and percentage of total elongation at maximum force and yield strain, respectively. In Table 2, CRB550 denotes the cold-rolled ribbed rebar with a nominal tensile strength of 550 MPa, and was used as secondary constructional reinforcement; HRB400 and HRB500 are hot-rolled ribbed rebars, and were used as primary carrying reinforcement.

3.4 Test setup, load scheme and instrumentation

Figure 3 shows the test setup, where the specimen was securely clamped to the reaction floor and subjected to cyclic lateral loading under constant axial load N (Table 1). The axial load ratios $N/(A_w f_{c,m})$ were about 0.07 for all specimens, where A_w denotes the gross cross-sectional area of wall. The vertical jack could move freely in the horizontal direction to accommodate the top lateral displacement. The lateral cyclic loading was displacement controlled. The displacement was expressed in terms of the drift ratio θ, which was defined as the ratio of the top lateral displacement Δ (monitored by the displacement transducer D1 in Fig. 3) over the height of D1 relative to the wall base (= 2070 mm). θ increased in the sequence of 1/2000, 1/1000, 1/660, 1/500, 1/300, 1/200, 1/150, 1/100, 1/66, and 1/50. One cycle was applied before 1/500 drift, while three cycles (two cycles for CS1.2H) were applied after that. The height H of the lateral loading point (i.e., the centroid of the loading beam) relative to the wall base was 2070 mm. In each loading cycle, a push was exerted first, followed by a pull, where the push was defined as positive loading and the pull as negative loading. The test was terminated when the axial load could not be maintained or the lateral load decreased below half of the maximum load.

Strain gauges (SGs) were mounted on longitudinal and horizontal rebars to monitor strain responses at various locations. As shown in Fig. 3, displacement transducers (DTs) were used to study various deformation responses of specimens, such as the top lateral displacement Δ, shear slippage and opening deformation of vertical and horizontal joints, and slippage or rotation of foundation beam.

Table 2 Material properties of rebars

Type	Grade	$f_{y,m}$ (MPa)	$f_{u,m}$ (MPa)	A_{gt} (%)	ε_y ($\times 10^{-6}$)
C6	CRB550	484.8	677.5	9.7	2424
D8	HRB400	466.1	666.6	9.1	2331
D10	HRB400	502.0	678.7	9.8	2510
E20	HRB500	579.9	762.1	11.7	2900
E28	HRB500	561.1	729.4	11.1	2806

4 Test results

The main results of all specimens are summarized in Table 3, where HRY hereinafter denotes the point when horizontal rebars yielded by tension; the effective yield point was generated from the idealized force-displacement curve outlined in ASCE 41-17 (2017); the ultimate point was taken as the point corresponding to

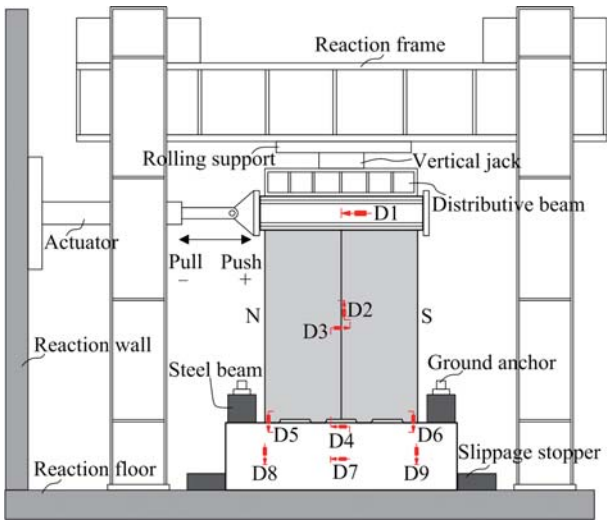

Fig. 3 Test setup and instrumentation

Table 3 Main test results of specimens

Specimen	Load direction	HRY		Effective yield		Peak load		Ultimate	μ_Δ	F_F (kN)	$\frac{F_{Ry}}{F_p}$	$\frac{F_p}{f_{c,m}b_w h_w}$	$\frac{F_p}{v_n^{JGJ}}$	$\frac{F_p}{v_n^{ACI}}$	$\frac{F_p}{v_n^{Kassem}}$
		F_{Ry} (kN)	θ_{Ry}	F_y (kN)	θ_y	F_p (kN)	θ_p	θ_u							
CS1.2	(+)	892.8	1/462	1122.7	1/514	1366.4	1/143	1/64	8.8	1439.7	0.65	0.157	1.87	1.58	1.35
	(-)	802.6	1/242	811.7	1/613	1162.4	1/102	1/63			0.69	0.133	1.59	1.34	1.15
	Avg	847.7	1/317	967.2	1/559	1264.4	1/119	1/63			0.67	0.145	1.73	1.46	1.25
CS1.2H	(+)	499.4	1/435	543.2	1/529	685.7	1/200	1/42	10.1	1334.3	0.73	0.096	1.33	1.14	1.41
	(-)	505.6	1/571	581.2	1/550	746.8	1/241	1/73			0.68	0.104	1.45	1.24	1.53
	Avg	502.5	1/494	562.2	1/539	716.3	1/219	1/54			0.70	0.100	1.39	1.19	1.47
CD1.3	(+)	685.3	1/241	770.0	1/428	1033.0	1/101	1/60	7.1	1194.9	0.66	0.143	1.63	1.37	1.28
	(-)	486.5	1/587	780.0	1/451	966.3	1/103	1/63			0.50	0.134	1.52	1.28	1.19
	Avg	585.9	1/342	775.0	1/439	999.7	1/102	1/62			0.59	0.138	1.58	1.32	1.24
PD1.3	(+)	749.5	1/227	806.1	1/392	1020.4	1/70	1/61	6.7	1191.6	0.73	0.142	1.75	1.35	1.32
	(-)	671.1	1/244	832.0	1/385	1046.4	1/95	1/55			0.64	0.145	1.79	1.38	1.35
	Avg	710.3	1/235	819.1	1/389	1033.4	1/81	1/58			0.69	0.143	1.77	1.37	1.33
PD1.3S	(+)	648.0	1/416	914.0	1/379	1143.7	1/100	1/51	6.5	1192.7	0.57	0.150	1.93	1.49	1.43
	(-)	669.4	1/332	843.0	1/383	1109.8	1/101	1/68			0.60	0.146	1.87	1.45	1.39
	Avg	658.7	1/370	878.5	1/381	1126.8	1/100	1/59			0.58	0.148	1.90	1.47	1.41
PT1.0	(+)	1037.1	1/262	1199.0	1/432	1459.4	1/100	1/59	7.2	1698.1	0.71	0.154	1.92	1.53	1.32
	(-)	965.0	1/224	1121.1	1/445	1370.1	1/103	1/63			0.70	0.145	1.80	1.43	1.24
	Avg	1001.1	1/241	1160.1	1/438	1414.8	1/102	1/61			0.71	0.150	1.86	1.48	1.28

a 20% reduction in lateral load resistance; the shear-compression ratio $F_p/(f_{c,m}b_w h_w)$ was used to remove the effect of the concrete strength and cross-sectional area. Table 3 shows that the loads corresponding to horizontal rebars yielding accounted for 0.50–0.73 of peak loads.

4.1 Specimens CS1.2 and CS1.2H

Figure 4 shows test results of CS1.2 and CS1.2H. VRY in Fig. 4(c) hereinafter denotes the point when extreme boundary longitudinal rebars yielded by tension. The secant stiffness K is defined as $K = F/\Delta$ (Fig. 4(d)), and the initial stiffness K_0 is obtained from linearly fitting the curve of F against Δ at the loading cycle of 1/2000 drift. Considering the strength differences of specimens, the equivalent viscous damping ratio h_e is used to evaluate the relative energy dissipation capacity of all specimens for better comparisons. As shown in Fig. 4(e), h_e is obtained as the ratio between the hysteretic energy and the corresponding elastic energy of the equivalent viscous system.

For CS1.2, horizontal flexural cracks appeared at a height of 0–700 mm from the wall base under 1/1000 drift, and then inclined cracks developed with horizontal cracks barely developing; a set of crisscross diagonal cracks formed under 1/500 drift; horizontal distributed rebars of precast panels (HDRP) yielded by tension under 1/200 drift; crisscross inclined cracks covered the whole wall under 1/150 drift; the extreme boundary longitudinal rebars yielded by tension near peak loads; under 1/50 drift, inclined cracks widened quickly, and obvious shear slippage formed at the boundary vertical joints (BVJs) connecting the precast panel and CBE; and finally, the bottom concrete at the terminal of diagonal cracks (i.e., concrete in compression-shear zone) crushed under compression-shear, resulting in quite rapid strength degradation. The concrete crushing zone was continuously distributed in precast panels and CBEs, indicating that precast panels and CBEs could work together under compression-shear. After testing and removal of the outer wythes of the precast panel, it was observed that inclined cracks of the outer wythes, concrete ribs of precast panel, and inside cast-in situ concrete extended along the same directions (Fig. 4(b)), indicating that the precast panels and inside cast-in situ concrete could work together. In addition, a vertical crack developed along one vertical constructional rebar of the precast panel under 1/100 drift (Fig. 4(a)), due to the thinner concrete cover, and shear slippage was observed around this vertical crack.

Due to the absence of cast-in situ concrete in middle vertical holes, CS1.2H failed in a mode significantly different from CS1.2, characterized by obvious cracking at the two hollow vertical holes (Fig. 4(a)). These vertical cracks formed under 1/1000 drift, and obvious shear slippage developed around these vertical cracks under 1/300 drift. HDRP within the vertical hole region yielded by tension under 1/300 drift, earlier than CS1.2.

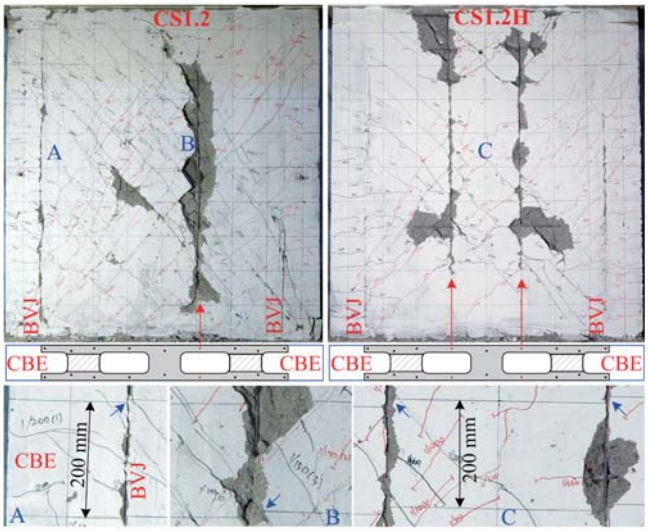

(a) Damage feature after first cycle of 1/50 drift

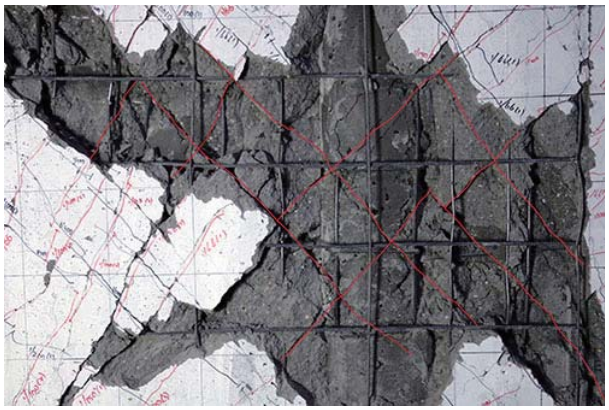

(b) Crack distribution on precast and cast-in-situ concrete for CS1.2

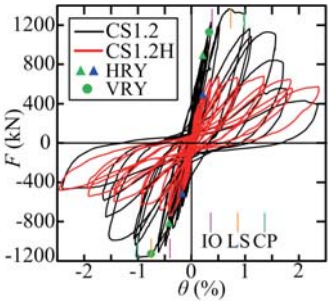

(c) Hysteretic loops

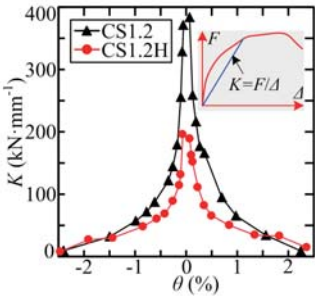

(d) Stiffness degradation

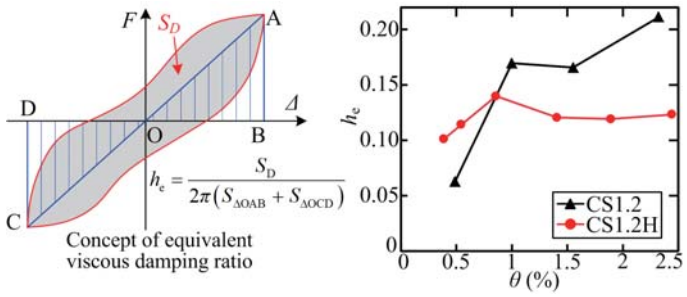

(e) Energy dissipation

Fig. 4 Results of Specimens CS1.2 and CS1.2H

Afterwards, CS1.2H was divided into three parts by these vertical cracks (Fig. 4(a)), and failed in a deformation pattern similar to slit concrete walls (Kwan *et al.*, 1994), achieving more gentle post-peak strength degradation compared with CS1.2 (Fig. 4(c)). In addition, CS1.2H exhibited asymmetric hysteretic behavior at the post-peak stage due to the different development process of these two vertical cracks. Obvious shear slippage formed around these vertical cracks at the post-peak stage, resulting in pinched hysteresis loops and decreasing h_e (Fig. 4(e)). Under 1/1000 and 1/300 drift, the maximum crack width for CS1.2H were 0.25 and 0.80 mm, respectively, and 0.05 and 0.40 mm for CS1.2. This reveals that CS1.2H performed worse in cracking control.

The shear-compression ratio $F_p/(f_{c,m}b_w h_w)$ and the initial stiffness K_0 of CS1.2 were 1.45 and 1.97 times that of CS1.2H, respectively. Figure 4(d) shows that the secant stiffness K of CS1.2 was significantly greater than CS1.2H prior to peak loads. Note that weak sections formed at vertical holes without inside cast-in situ concrete, and CS1.2H reached horizontal rebar yielding and peak loads earlier than CS1.2. These indicate that inside cast-in situ concrete could significantly improve the strength and stiffness of EVE walls. Bare precast panel without inside cast-in situ concrete may not be used as primary lateral resistant members in high-rise structures, due to its poor cracking, strength and stiffness behavior. Conversely, taking ultimate drift θ_u to evaluate the deformation capacity of specimen, CS1.2H achieved excellent deformation capacity (mean of θ_u = 1/54), so using bare precast panels as secondary walls may be a viable option in EVE-PHSW.

4.2 Specimens CD1.3, PD1.3 and PD1.3S

Figure 5 shows test results of CD1.3, PD1.3 and PD1.3S, which consisted of two precast panels. These three specimens underwent a similar failure process. Horizontal flexural cracks appeared under 1/660 drift, and afterwards, inclined cracks developed and extended gradually; macroscopic shear slippage formed at the middle vertical joints (MVJs) connecting adjacent precast panels under 1/300 drift; horizontal rebars yielded by tension under 1/300 or 1/200 drift; crisscross inclined cracks covered the whole wall under 1/200 drift, while shear slippage developed at BVJs of CD1.3; the extreme boundary longitudinal rebars yielded by tension near peak loads under 1/100 drift; under 1/66 drift, concrete slightly spalled, and vertical cracks similar to CS1.3 formed at vertical holes of CD1.3 and PD1.3 (Fig. 5(a)); under 1/50 drift, inclined cracks widened quickly, and lateral loads degraded rapidly due to concrete in the compression-shear zones crushing.

Note that crack distributions of these three specimens showed slight differences. Early boundary horizontal cracks of CD1.3 extended 200 mm long to the BVJs and then developed into inclined cracks, while 400 mm long horizontal cracks developed for PD1.3 and PD1.3S, indicating that the BVJ connecting the CBE and precast panel had an influence on crack patterns. However, the measured strength (i.e., the peak lateral load) of PD1.3

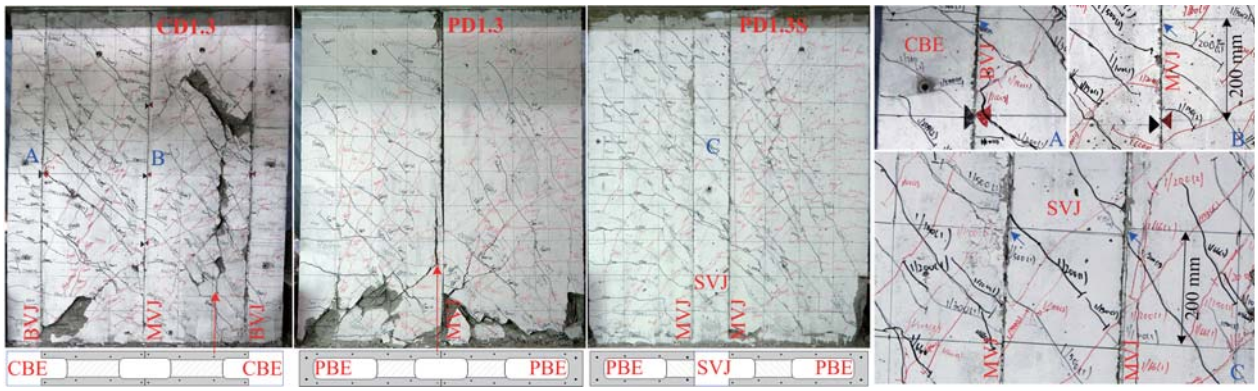

(a) Damage feature after first cycle of 1/50 drift

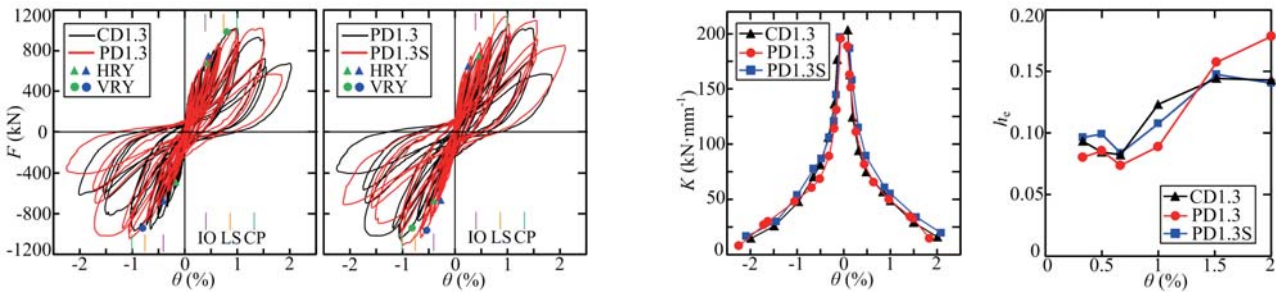

(b) Hysteretic loops (c) Stiffness degradation (d) Energy dissipation

Fig. 5 Results of Specimens CD1.3, PD1.3 and PD1.3S

was only 3.4% higher than CD1.3, revealing that details of boundary elements (PBE or CBE) had little effect on the strength of squat EVE walls.

For CD1.3, PD1.3 and PD1.3S, most inclined cracks on one precast panel could not continuously extend into the adjacent panel but extended along the MVJ to a certain length. In particular, inclined cracks of PD1.3S, in which the two precast panels were connected by a SVJ, delivered a better continuity than that of CD1.3 and PD1.3. In addition, the measured strength of PD1.3S was 9.0% and 12.7% higher than that of PD1.3 and CD1.3, respectively. These reveal that the force transfer performance of SVJ was slightly better than CVJ.

As shown in Table 3, θ_p (except θ_p of PD1.3 in positive direction) and θ_u of CD1.3, PD1.3 and PD1.3S were almost identical. K_0 of CD1.3, PD1.3 and PD1.3S were 236.4, 233.5 and 246.6 kN/mm, respectively, and these three specimens exhibited similar stiffness degradation behavior (Fig. 5(c)). h_e of these three specimens were similar before 1/66 drift. However, compared with PD1.3, CD1.3 and PD1.3S, they had more vertical joints, and exhibited a slightly decreasing h_e under 1/50 drift due to shear slippage at vertical joints (Fig. 5(d)). In summary, the details of boundary elements (CBE or PBE) and vertical joints (CVJ or SVJ) had little effect on hysteretic characteristics, deformation capacity, stiffness and energy dissipation of EVE walls. SVJ exhibited slightly better force transfer performance with more continuously inclined crack distributions and slightly higher strength of walls.

4.3 Specimen PT1.0

Figure 6 shows test results of PT1.0, which consisted of three precast panels. The failure process of PT1.0 was similar to that of PD1.3 and PD1.3S. Macroscopic shear slippage formed at MVJs under 1/300 drift; horizontal rebars yielded by tension under 1/200 drift; the extreme boundary longitudinal rebars yielded by tension under 1/150 or 1/100 drift in the positive or negative direction, respectively; under 1/66 and 1/50 drift, inclined cracks widened quickly, and lateral loads degraded rapidly due to concrete crushing in the compression-shear zones. After test and removal of the outer wythes of the precast panels, it was observed that the concrete crushing zone was continuously distributed in the three precast panels (Fig. 6(a)), indicating that they could work together under compression-shear.

5 Discussion

5.1 Design implication and global performance evaluation

5.1.1 Shear strength

Comparisons between the measured strength F_p and calculated flexural strength F_F for all specimens are summarized in Table 3, where F_F was calculated by the conventional theory of reinforced concrete sections subjected to combined bending moment and axial compression. Table 3 shows that the measured strength of each specimen was lower than the calculated flexural strength. In addition, all specimens were dominated by shear cracks, and horizontal rebars yielded before extreme boundary longitudinal rebars. It can be concluded that all specimens failed in shear mode, and the lateral load resistance could be estimated from the shear strength of the walls.

Shear strength is a key parameter in the design of squat walls. Accurately predicting the shear strength of concrete walls has attracted a lot of research in the past few decades. Various models have been developed, such as the softened truss model (Mau and Hsu, 1987), softened strut-and-tie model (Hwang *et al.*, 2001) and UCSD shear model (Kowalsky and Priestley, 2000). However, existing models have limitations and showed substantial scatter compared to experimental results from different literature (Kassem, 2015). Considering the complexity of this issue and scattered predictions from different physically-based models, most design codes estimate shear strength of cast-in situ walls based on empirical equations, which have been kept constant for decades. In addition, the vertical joints and precast to cast-in situ concrete interfaces make it more difficult to accurately predicate the shear strength of EVE walls. If the design equations for cast-in situ walls can be used to estimate the shear strength of EVE walls, the design of EVE walls will be greatly simplified. Thus, three

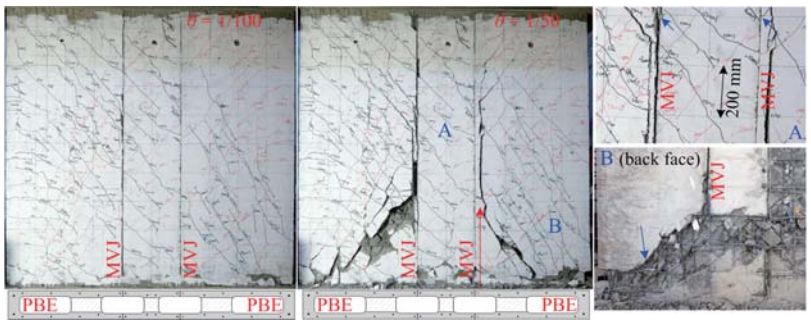

(a) Crack distribution and failure mode

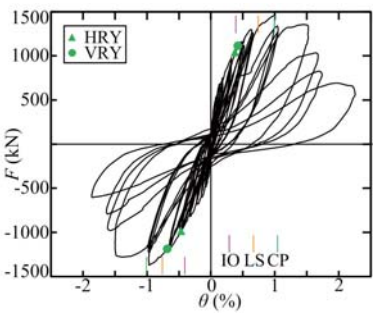

(b) Hysteretic loops

Fig. 6 Results of Specimen PT1.0

sets of shear strength formulas provided in the Chinese code JGJ 3-2010 (2010), Section 18.10 of ACI 318-14 (2014) and Kassem (2015) are discussed to verify their applicability for EVE walls. JGJ 3-2010 and ACI 318-14 consider the shear strength as the sum of concrete contribution and web reinforcement contribution.

According to JGJ 3-2010, the shear strength of rectangular cast-in situ walls is given by
for monotonic loading,

$$V_{\mathrm{n}}^{\mathrm{JGJ\text{-}m}}=\frac{1}{\lambda-0.5}\left(0.5f_{\mathrm{t}}t_{\mathrm{w}}h_{\mathrm{w0}}+0.13N\right)+f_{\mathrm{yh}}\rho_{\mathrm{h}}t_{\mathrm{w}}h_{\mathrm{w0}} \quad (1a)$$

for cyclic loading, $$V_{\mathrm{n}}^{\mathrm{JGJ\text{-}c}}=0.8V_{\mathrm{n}}^{\mathrm{JGJ\text{-}m}} \quad (1b)$$

where f_{t} = tensile strength of concrete; t_{w} = wall thickness; h_{w0} = effective depth of wall section; N = axial compressive; f_{yh} = yield strength of horizontal web reinforcement; ρ_{h} = horizontal web reinforcement ratio; and $\lambda = M/(Vh_{\mathrm{w0}})$ denotes the moment-to-shear ratio of wall. In Eq. (1), the lower bound value of λ is limited to 1.5 (i.e., it is assumed to be equal to 1.5 if it is smaller than 1.5).

For seismic design of special structural walls with rectangular cross-sections, the equation in Section 18.10 of ACI 318-14 can be written as:

$$V_{\mathrm{n}}^{\mathrm{ACI}}=A_{\mathrm{w}}\left(\alpha_{\mathrm{c}}\sqrt{f_{\mathrm{c}}'}+\rho_{\mathrm{h}}f_{\mathrm{yh}}\right)\le 0.83A_{\mathrm{w}}\sqrt{f_{\mathrm{c}}'} \quad (2)$$

where f_{c}' = concrete compressive strength; the aspect ratio dependent coefficient $\alpha_{\mathrm{c}}=0.25$ for $H/h_{\mathrm{w}}\le 1.5$, 0.17 for $H/h_{\mathrm{w}}\ge 2$ and varies linearly for $1.5\le H/h_{\mathrm{w}}\le 2$.

Kassem (2015) developed a closed-form equation for shear strength of cast-in situ walls based on the strut-and-tie model, which considers the contribution of concrete, horizontal web reinforcement and vertical web reinforcement through three load paths. The equation parameters were calibrated using test results in existing literature. The proposed closed-form equation is as follows:

$$V_{\mathrm{n}}^{\mathrm{Kassem}}=0.27f_{\mathrm{c}}'t_{\mathrm{w}}d_{\mathrm{w}}\cdot\left[\psi k_{\mathrm{s}}\sin\left(2\alpha\right)+0.11\omega_{\mathrm{h}}\frac{H}{d_{\mathrm{w}}}+0.30\omega_{\mathrm{v}}\cot\left(\alpha\right)\right]\le 0.83t_{\mathrm{w}}d_{\mathrm{w}}\sqrt{f_{\mathrm{c}}'} \quad (3)$$

where d_{w} = horizontal length between the tensile and compressive forces in boundary elements; ψ = 0.95-f_{c}'/250; k_{s} = ratio of the horizontal length of the compressive zone at the wall base to d_{w}; the diagonal strut angle $\alpha=\tan^{-1}(H/d_{\mathrm{w}})$; and the horizontal or vertical web reinforcement index is calculated as $\omega=(\rho f_{\mathrm{y}})/f_{\mathrm{c}}'$, in which ρ and f_{y} denote the reinforcement ratio and yield strength of horizontal or vertical web reinforcement.

Experimental databases of cast-in situ concrete walls have been developed by Gulec (2009), Sánchez-Alejandre (2009) and Kassem (2015). 275 rectangular walls that failed in shear were selected from these databases for further analysis. The t_{w}, H/h_{w}, ω_{h}, ω_{v} and $N/(A_{\mathrm{w}}f_{\mathrm{c}}')$ of these walls were 23–200 mm, 0.3–2.1, 0–0.2, 0–0.2 and 0–0.42, respectively, while those of EVE walls in this study were 200 mm, 1.0–1.3, 0.048–0.052, 0–0.073 and 0.07. Comparisons between the test shear strength V_{test} (i.e., F_{p}) and the calculated shear strength V_{n} generated from Eqs. (1)–(3), together with the corresponding average (Avg), standard deviation (SD) and coefficient of variation (CoV) of $V_{\mathrm{test}}/V_{\mathrm{n}}$, are shown in Fig. 7 and Table 3. The measured-to-evaluated strength ratios $V_{\mathrm{test}}/V_{\mathrm{n}}^{\mathrm{JGJ}}$, $V_{\mathrm{test}}/V_{\mathrm{n}}^{\mathrm{ACI}}$, and $V_{\mathrm{test}}/V_{\mathrm{n}}^{\mathrm{Kassem}}$ of EVE wall specimens are 1.39~1.90, 1.19~1.48, and 1.24–1.47, respectively, indicating that JGJ 3-2010 (2010), ACI 318-14 (2014) and Kassem (2015) equations provide conservative predictions of the shear strength of EVE walls. For conventional cast-in situ walls, the predication generated from JGJ 3-2010 (2010), ACI 318-14 (2014) and Kassem (2015) shows substantial scatter, with CoV of 0.41, 0.45 and 0.51, respectively, revealing the complexity of shear strength of cast-in situ walls. Overall, the strength ratios $V_{\mathrm{test}}/V_{\mathrm{n}}^{\mathrm{JGJ}}$, $V_{\mathrm{test}}/V_{\mathrm{n}}^{\mathrm{ACI}}$, and $V_{\mathrm{test}}/V_{\mathrm{n}}^{\mathrm{Kassem}}$ for EVE wall specimens were not smaller than the Avg of these for cast-in situ walls with similar H/h_{w}. Therefore, the shear strength equations for cast-in situ walls in JGJ 3-2010 (2010), ACI 318-14 (2014) and Kassem (2015) can be conservatively used for estimating the shear strength of EVE walls, achieving a strength reserve comparable to cast-in situ walls.

In addition, underestimating the shear strength of EVE walls will lead to two advantages: (1) the underestimation of the shear-to-flexural strength ratio and (2) the increase of horizontal additional spliced rebars (HASR) in vertical joints. Underestimating the shear-to-flexural strength ratio is conservative because it results in a higher amount of horizontal web reinforcement and decreases the probability of brittle shear failure. Simultaneously, the larger amount of horizontal web reinforcement means the increase of corresponding HASR, which will enhance the vertical joints and postpone damage to vertical joints.

5.1.2 Deformation capacity

Deformation capacity represents the capacity of the specimen to develop nonlinear deformation without extensive strength degradation. Herein, the deformation capacity of the specimen was evaluated by the ultimate drift θ_{u} and the displacement ductility ratio μ_{Δ} (= $\theta_{\mathrm{u}}/\theta_{\mathrm{y}}$, Table 3). According to ASCE 41-17 (2017), component ductility demands can be classified as low, moderate, or high when $\mu_{\Delta}<2$, $2\le\mu_{\Delta}\le 4$, or $\mu_{\Delta}>4$, respectively. It shows that all specimens can be classified as high-ductile components with μ_{Δ} ranging

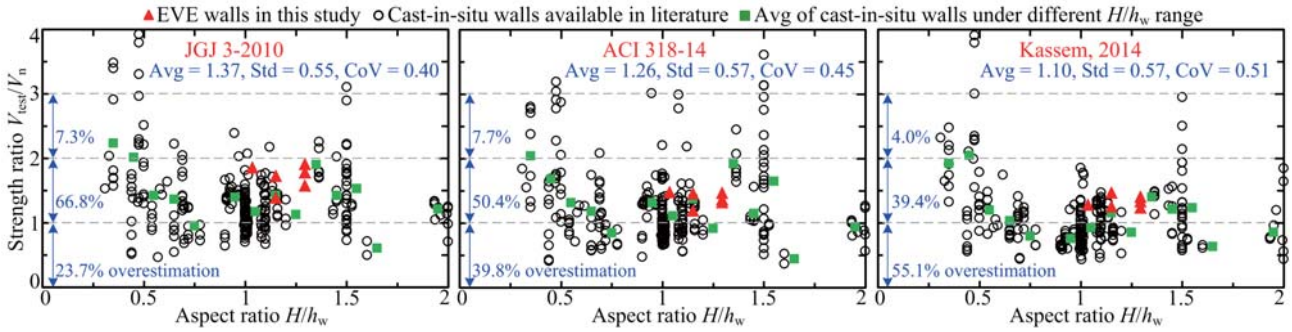

Fig. 7 Comparison of strength ratio V_{test}/V_n for EVE walls and cast-in situ walls using different equations

from 6.5 to 10.1. Figure 8 compares the ultimate drift θ_u of EVE walls in this study and cast-in situ walls from the abovementioned databases. θ_u of EVE wall specimens ranged from 1/63 to 1/54, which were much larger than 1/120 (i.e., the limiting elasto-plastic drift for structural walls stipulated in JGJ 3-2010 (2010)). Overall, θ_u of EVE walls were slightly larger than that of cast-in situ walls, indicating that EVE walls achieved deformation capacity comparative to cast-in situ walls.

5.1.3 Effective lateral stiffness

Effective lateral stiffness is a key modeling parameter that has a significant effect on the system response in structural analysis. Considering the effect of concrete cracking and bond slippage, ASCE 41-17 (2017) recommends a flexural rigidity of $0.35E_cI_g$ and a shear rigidity of $0.4E_cA_w$ for cracked cast-in situ walls, where E_cI_g and E_cA_w denote the gross flexural and shear stiffness of the wall section, respectively. However, for precast walls, the deformation of vertical and horizontal joints may affect the effective lateral stiffness. Thus, the applicability of recommended effective stiffness for monolithic cast-in situ walls should be thoroughly examined. Table 4 summarizes the measured effective lateral stiffness K_{eff} and the calculated effective lateral stiffness K_c. K_{eff} was derived by the idealized force-displacement procedure outlined in ASCE 41-17. Note that the lateral displacement Δ mainly consists of the flexural and shear deformation components, both flexural and shear stiffness have been considered in the calculation of K_c, with the recommended $0.35E_cI_g$ for flexural stiffness and $0.4E_cA_w$ for shear stiffness. The ratios K_{eff}/K_c ranged from 1.07 to 2.09, validating that the recommended effective stiffness for monolithic cast-in situ walls in ASCE 41-17 can be used for EVE walls. K_{eff}/K_c of CS1.2H is much larger than that of the rest specimens, since only the two outer wythes of the precast panel were considered in the calculation of K_c.

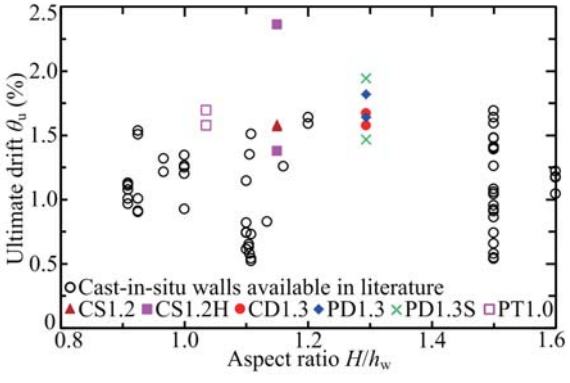

Fig. 8 Comparison of ultimate drift for EVE walls and cast-in situ walls

5.1.4 Global performance evaluation

The behavior of joints connecting precast panels and internal precast to cast-in situ concrete interfaces in EVE walls, especially the shear slippage in vertical joints and vertical cracks, results in global performance that differ somewhat from conventional cast-in situ walls. Figure 9 shows that the shear slippage δ_v at BVJs were significantly smaller than δ_v at MVJs, consistent with the shear stress distribution along the wall cross-section. For CD1.3, PD1.3, PD1.3S, and PT1.0, δ_v at MVJs developed slowly before 1/300 drift, and increased rapidly after 1/300 or 1/200 drift. For instance, δ_v at MVJs ranged from 0.43 to 1.29 mm under 1/300 drift, and 4.06 to 5.42 mm under 1/100 drift (around peak loads). EVE walls could be considered as a whole and behaved like conventional cast-in situ walls before 1/300 drift, since the slippage at vertical joints and vertical cracks were rather small. After this drift, the EVE specimens exhibited behavior between conventional cast-in situ walls and slit walls with slippage at vertical joints and the development of vertical cracks. The common main diagonal cracks (Fig. 10) and brittle shear failure in conventional cast-in situ walls have been avoided in EVE walls, which were full of crisscross inclined cracks with uniform width and exhibited moderate strength degradation. In addition, for EVE walls with inside cast-in situ concrete, the equivalent viscous damping ratio h_e under 0.01 and 0.02 drift were 0.09–0.17 and 0.14–0.18, respectively.

Table 4 Effective lateral stiffness of specimens

Specimen	CS1.2	CS1.2H	CD1.3	PD1.3	PD1.3S	PT1.0
K_{eff} (kN/mm)	260.1	145.2	163.5	153.1	161.8	243.1
K_c (kN/mm)	186.1	69.5	132.1	132.7	138.3	228.0
K_{eff}/K_c	1.40	2.09	1.24	1.15	1.17	1.07

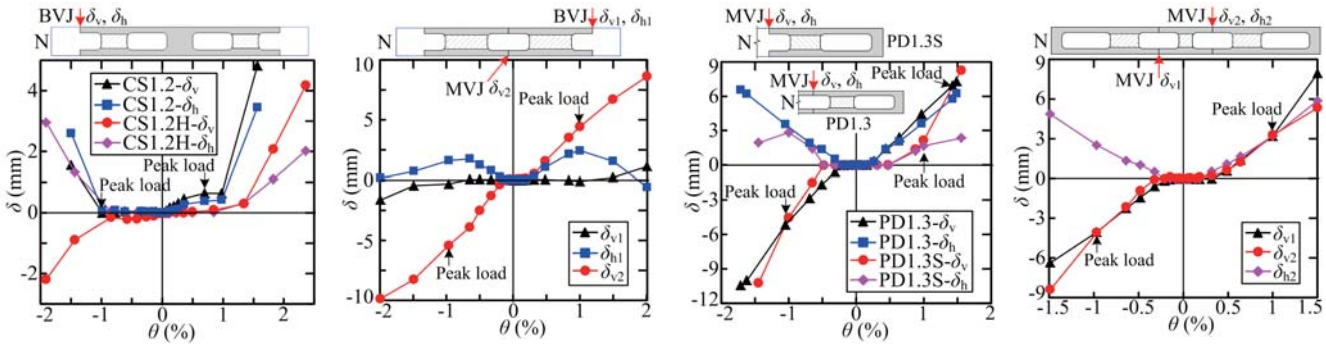

(a) CS1.2 and CS1.2H (b) CD1.3 (c) PD1.3 and PD1.3S (d) PT1.0

Fig. 9 Measured shear slippage δ_v and horizontal opening deformation δ_h at vertical joints

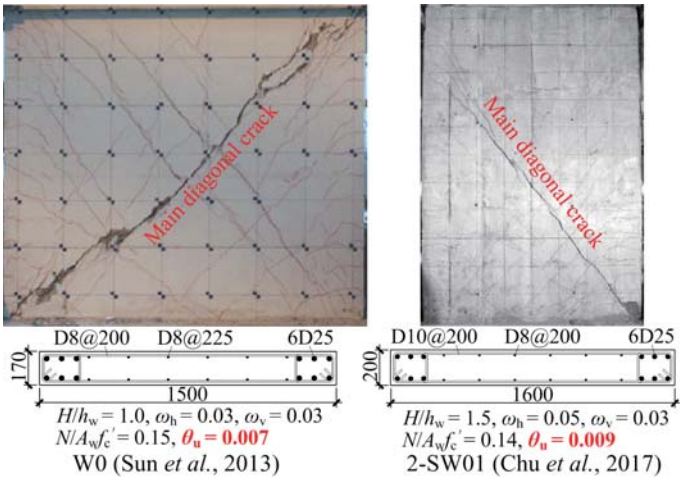

Fig. 10 Crack pattern of cast-in situ walls in literature

For squat cast-in situ walls tested by Ji *et al.* (2018) and Peng *et al.* (2015), h_e under 0.01 and 0.02 drift were 0.09–0.12 and 0.11–0.13, respectively. These indicate that EVE walls exhibited energy-dissipation ability comparable to cast-in situ walls, especially under large drift. Compared with squat cast-in situ walls, EVE walls delivered greatly improved deformation capacity (Fig. 8), and were capable of maintaining comparative shear strength reserve (Fig. 7) as well as energy-dissipation ability.

The performance level of EVE walls can be evaluated by code-based damage limits for cast-in situ walls. For shear-dominated structural walls with axial load ratios exceeding 0.05, ASCE 41-17 (2017) proposes 0.004, 0.0075 and 0.01 as the acceptable drifts for Performance Level of Immediate Occupancy (IO), Life Safety (LS) and Collapse Prevention (CP), respectively, which are illustrated in hysteretic loops through Fig. 4 to Fig. 6. As specified in the Chinese code GB 50011-2010 (2010), the seismic-resisting target for structural walls is no damage, repairable and no collapse under frequent, precautionary and rare earthquakes, which corresponds to 63.2%, 10% and 2% probability of exceedance in 50 years, and a maximum allowable interstory drift of 1/1000, 1/300 and 1/120, respectively. As observed from the tests, for specimens with inside cast-in situ concrete, under 0.0001 drift, specimens suffered hairline flexural cracking (< 0.05 mm width); under 0.004 drift, specimens were dominated by inclined cracks (< 0.5 mm width), and horizontal rebars suffered tension yielding or approached yielding; under 0.01 drift, specimens suffered extensive cracking but no spalling, and could continue to resist axial and lateral loads. It can be concluded that EVE walls satisfied the Performance Level requirement in ASCE 41-17 (2017) and the seismic-resisting target in GB 50011-2010 (2010) for cast-in situ walls.

5.2 Performance of noncontact lap splice

NLSs are used to transfer the stress of HDRP to corresponding HASR in MVJs or BVJs, which transfer the forces from one precast panel to an adjacent precast panel or CBE. The deformation at vertical joints (Fig. 9) and the shear stress distribution along the wall cross-section indicate higher force transfer demands in MVJs compared to BVJs. Thus the performance of NLSs in MVJs is discussed as follows.

Strain responses of HASR and HDRP within the overlapping region were monitored by strain gauges that were mounted at the middle and end of the overlapping region. Figures 11, 12 and 13 illustrate the strain skeleton curves, strain distribution along the splice length and

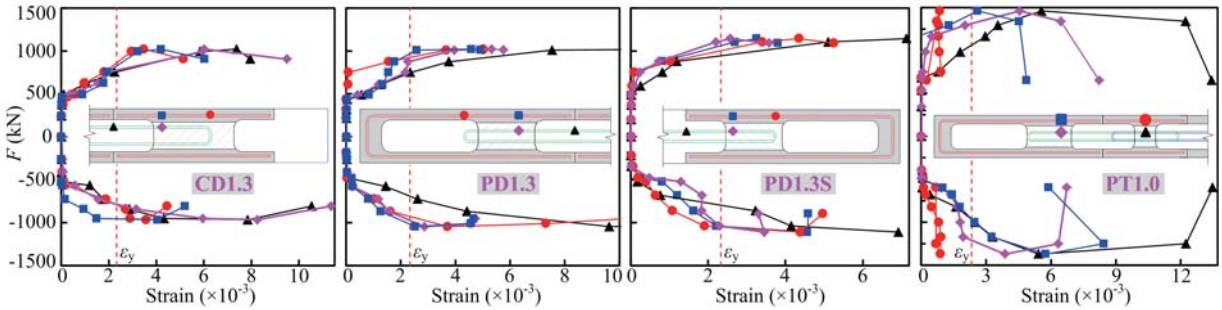

Fig. 11 Strain skeleton curves of rebars within the overlapping region at MVJs

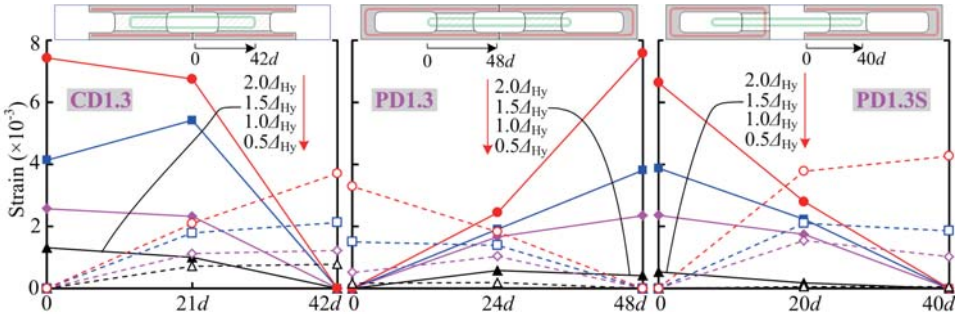

Fig. 12 Horizontal rebar strain distribution along splice length at MVJs

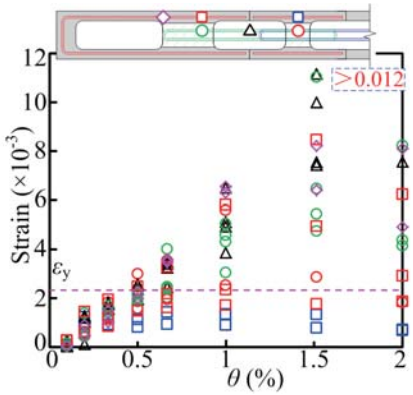

Fig. 13 Horizontal rebar strain for PT1.0

maximum strains under applied drift of HASR and HDRP, respectively. In Fig. 12, solid lines and dashed lines denote strains on HASR and HDRP, respectively, and Δ_{Hy} corresponds to the lateral displacement when HASR yielded by tension.

Figure 11 shows that both strains on HASR and HDRP within the overlapping region increased with lateral loads, and no abrupt strain decrease was observed. HASR or HDRP suffered tension yielding under 1/300 or 1/200 drift, and almost all strain monitor points underwent extensive yielding prior to peak loads. Strains on HDRP decreased along the spliced length, and simultaneously, strains on HASR increased along the spliced length (Fig. 12), revealing the presence of the force transfer between HDRP and HASR. The profiles of strain versus the splice length were similar to those obtained from tests of NLSs in pure tension (McLean and Smith, 1997). However, unlike NLSs in pure tension, horizontal rebar stress in walls was significantly influenced by the distribution and opening of inclined cracks, resulting in different strains on HASR and HDRP at the end of the overlapping region. Furthermore, under ultimate states, concrete within the overlapping region was dominated by inclined cracks resembling adjacent zones of the wall, and no concentrated transverse crack was observed. The rebar strains and crack patterns indicate that NLSs in vertical joints with l_d = 1.0–1.2l_{aE} and s = 4.5–6.0d could enable the specimens to exhibit stable load-carrying capacity through extensive deformations.

Figure 13 also shows that the maximum strains at the overlapping region end (corresponding to the position of vertical joints) of HASR, the overlapping region center of HASR, the overlapping region end of HDRP, and the overlapping region center of HDRP decreased in turn under the same drift. This indicates that HASR might contribute more to shear-resistance compared with HDRP at MVJs. For Specimen PT1.0, which consisted of three precast panels, strains on HDRP in the middle precast panel were significantly smaller than the corresponding HASR, and no yielding was observed, indicating that the forces in HASR of the south vertical joint were directly transferred to HASR of the north vertical joint by lapping, bypassing HDRP in the middle precast panel.

The force transfer between HDRP and HASR can be explained in terms of the transfer of forces via the plane truss model (Sagan *et al.*, 1988) shown in Fig. 14. Tension

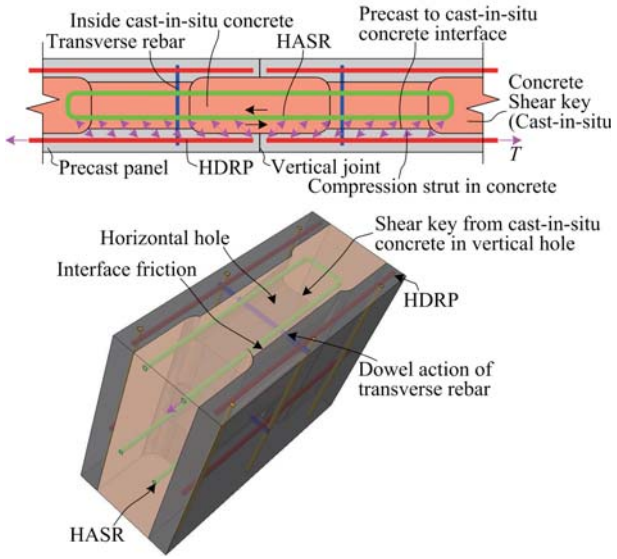

Fig. 14 Force transfer mechanism of NLS at MVJs

in rebars causes radial outward pressure on the concrete. The forces in HDRP of one precast panel are transferred by compression struts that form in concrete between the two spliced rebars and over to HASR. As more force is transferred from HDRP to HASR over the splice length, the strain distribution in Fig. 12 forms. The forces in HASR are transferred to HDRP of adjacent precast panel through a similar model, then the forces in HDRP in one side of the vertical joint are transferred to the HDRP in the other side. However, compared with NLSs in monolithic cast-in situ concrete, the force transfer in compression struts in EVE walls is more complex due to the presence of the precast to cast-in situ concrete interface. Compression struts cause shear and compression forces in the interface. The interface friction, dowel action of transverse rebars and shear key from the cast-in situ concrete in vertical holes together compose the shear resistance of the interface. Considering the complexity of these three components, the shear resistance of the interface V_R can be conservatively evaluated as a sum of the interface friction V_{Rf} and dowel action of transverse rebars V_{Rd}, neglecting the contribution of compression forces generated from the compression struts and shear key from the cast-in situ concrete in vertical holes. V_{Rf}, V_{Rd} and the shear demand of the interface V_D can be calculated as follows:

$$V_{Rf} = \tau A_c \tag{4a}$$

$$V_{Rd} = f_{yT} A_T / \sqrt{3} \quad \text{(Foerster } et\ al.\text{, 1989)} \tag{4b}$$

$$V_D = f_{yh} A_{sh} \tag{4c}$$

where A_c = area of concrete interface; f_{yT} = yield strength of transverse rebar; A_T = area of transverse rebar; and τ = bond strength of the interface under pure shear. A series of pure shear tests has been conducted to investigate the bond strength of the interface in EVE walls, showing that $\tau = 0.35$ MPa.

Taking Specimen PD1.3S with the shortest splice length ($l_d = 40d$) for instance, for a single HASR unit, $V_D = 23.4$ kN, $V_{Rf} = 22.4$ kN, and $V_{Rd} = 13.5$ kN. The ratio of V_R/V_D is 1.53, indicating that the precast to cast-in situ concrete interface could satisfy the shear transfer demand in NLSs. However, the estimation is over simplified, and further experimental and analytical study on this special problem is needed.

5.3 Shear-resistance performance of horizontal joint

The horizontal joint consists of the precast to cast-in situ superimposed interface and dowel rebars. Zhao *et al.* (2015) studied the shear-resistance mechanisms of the superimposed interface, showing that the strength capacity calculated by existing formulas exhibited remarkable differences, and the following formula provided reasonable prediction of shear strength of superimposed interfaces, with the mean of the measured-to-evaluated shear strength ratio for 29 specimens of 1.07.

$$V_u = 0.9[0.12 f_c A_c + 0.7(f_{yD} A_D + N)] \le 0.33 f_c A_c \text{ and } K_3 A_c \tag{5}$$

where f_{yD} = yield strength of dowel rebar; A_D = area of dowel rebar; and for ordinary concrete, $K_3 = 16.5$ MPa.

The slippage S at horizontal joints and the slippage-to-drift ratio S/Δ under peak load and ultimate states are summarized in Table 5, where the horizontal joint shear strength V_u was calculated by Eq. (5) with test material strengths. The maximum required-to-evaluated shear ratio F_p/V_u of all specimens ranged from 0.43 to 0.56. The slippage at the horizontal joint accounted for less than 4.9% and 2.6% of the top lateral displacement under peak load and ultimate states, respectively, revealing

Table 5 Slippage at horizontal joint

Specimen	Load direction	V_u (kN)	Peak load			Ultimate	
			F_p/V_u	S_p (mm)	S_p/Δ_p	S_u (mm)	S_u/Δ_u
CS1.2	(+)	2732	0.50	0.22	1.5%	0.12	0.4%
	(-)		0.43	0.83	4.1%	0.84	2.6%
CS1.2H	(+)	2718	0.25	0.01	0.1%	0.01	0.1%
	(-)		0.27	0.02	0.2%	0.09	0.3%
CD1.3	(+)	2161	0.48	0.22	1.0%	0.09	0.3%
	(-)		0.45	0.13	0.6%	0.07	0.2%
PD1.3	(+)	1853	0.55	0.17	0.6%	0.04	0.1%
	(-)		0.56	0.02	0.1%	0.16	0.4%
PD1.3S	(+)	2088	0.55	0.64	3.1%	0.19	0.5%
	(-)		0.53	0.49	2.4%	0.57	1.9%
PT1.0	(+)	2716	0.54	1.03	4.9%	0.57	1.6%
	(-)		0.50	0.16	0.8%	0.07	0.2%

that slippage at horizontals joint had a little effect on the global behavior of EVE walls. The horizontal joint exhibited a good slip-resisting ability, satisfying the dual requirements for force and deformation in EVE walls that failed in shear mode.

6 Conclusions

Based on an experimental study of six squat walls with EVE precast concrete hollow moulds, the following findings and conclusions are summarized.

(1) EVE wall specimens with inside cast-in situ concrete achieved the desired "strong bending and weak shear" and failed in shear mode, characterized by plenty of crisscross inclined cracks with uniform width, and vertical cracks along vertical constructional rebars. Shear slippage at vertical joints and vertical cracks after 0.005 drift prevented the common main diagonal cracks and brittle shear failure in squat cast-in situ walls.

(2) Inside cast-in situ concrete could significantly improve the shear strength and stiffness behavior of EVE walls. Bare precast panels without inside cast-in situ concrete may not be used as primary lateral resistant members in high-rise structures, due to their poor cracking, shear strength and stiffness behavior. However, bare panels can be used as secondary walls to utilize the excellent deformation capacity.

(3) Compared with squat cast-in situ walls, EVE walls delivered greatly improved deformation capacity with ultimate drift of 1/63–1/54, and were capable of maintaining comparative shear strength reserve and energy-dissipation ability. Both JGJ 3-2010 (2010) and ACI 318-14 (2014) provide conservative estimations of the shear strength of EVE walls, with measured-to-evaluated strength ratios of 1.39–1.90 and 1.19–1.48, respectively. The recommended effective stiffness for cast-in situ walls in ASCE 41-17 (2017) appeared to be appropriate for EVE walls. Failure processes indicated that EVE walls with inside cast-in situ concrete satisfied the Performance Level requirement in ASCE 41-17 (2017) and the seismic-resisting target in GB 50011-2010 (2010) for cast-in situ walls.

(4) Noncontact lap splices in vertical joints, which contribute to automated prefabrication and easy in situ erection, could enable EVE walls to exhibit stable load-carrying capacity through extensive deformations. The details of the precast to cast-in situ concrete interface could satisfy the shear transfer demand in noncontact lap splices.

(5) The details of boundary elements (cast-in situ or prefabricated) and vertical joints (contiguous or spaced) had little effect on the global behavior of EVE walls, except that the specimen with spaced vertical joints showed more continuously inclined crack distributions and slightly higher shear strength. The prefabricated boundary elements can be used in EVE walls for simplified situ construction.

(6) Slippage at horizontal joints, which accounted for less than 5% of the top lateral displacement, had little effect on the global behavior of EVE walls. The horizontal joint exhibited a good slip-resisting ability.

Acknowledgement

The authors express their sincere gratitude to Beijing Everest Green Building Technology Ltd. for the funding to support this study.

References

ACI 318-14 (2014), *Building Code Requirements for Structural Concrete and Commentary*, Farmington Hills, MI: American Concrete Institute.

ASCE 41-17 (2017), *Seismic Evaluation and Retrofit of Existing Buildings*, Reston, VA: American Society of Civil Engineers.

Cai L (2015), "Experimental Study on Seismic Behavior of Reinforced Concrete Composite Shear Wall," *M.D. Dissertation*, Tongji University, Shanghai. (in Chinese)

CEB-FIP Model Code 1990 (1990), *fib Model Code for Concrete Structures 1990*, Paris: International Federation for Structural Concrete (*fib*).

Chong X, Xie LL, Ye XG, Jiang Q and Wang DC (2016), "Experimental Study and Numerical Model Calibration of Full-scale Superimposed Reinforced Concrete Walls with I-Shaped Cross Sections," *Advances in Structural Engineering*, **19**(12): 1902–1916.

Chong X, Xie LL, Ye XG, Jiang Q and Wang DC (2017), "Experimental Study on the Seismic Performance of Superimposed RC Shear Walls with Enhanced Horizontal Joints," *Journal of Earthquake Engineering*, **21**(7): 1–17.

Chu MJ, Liu JL and Sun ZJ (2017), "Experimental Study on Mechanical Behaviors of New Shear Walls Built with Precast Concrete Hollow Moulds," *European Journal of Environmental and Civil Engineering*, **21**(7): 1–20.

Eurocode 2 (2004), *Design of Concrete Structures: Part 1-1: General Rules and Rules for Buildings*, London: British Standards Institution.

Foerster HR, Rizkalla SH and Heuvel JS (1989), "Behavior and Design of Shear Connections for Loadbearing Wall Panels," *PCI Journal*, **34**(1): 102–119.

GB 50010-2010 (2010), *Code for Design of Concrete Structures*, Beijing: China Ministry of Construction. (in Chinese)

GB 50011-2010 (2010), *Code for Seismic Design of Buildings*, Beijing: China Ministry of Construction. (in Chinese)

Gilbert RI and Kilpatrick AE (2015), "The Strength and Ductility of Lapped Splices of Reinforcing Bars in Tension," *Australian Journal of Structural Engineering*, **16**(1): 35–46.

Gulec CK (2009), "Performance-based Assessment and Design of Squat Reinforced Concrete Shear Walls," *Ph.D. Dissertation*, State University of New York at Buffalo.

Hamad BS and Mansour MY (1996), "Bond Strength of Noncontact Tension Lap Splices," *ACI Structural Journal*, **93**(3): 316–326.

Hwang SJ, Fang WH, Lee HJ and Yu HW (2001), "Analytical Model for Predicting Shear Strength of Squat Walls," *Journal of Structural Engineering*, **127**(1): 43–50.

JGJ 3-2010 (2010), *Technical Specification for Concrete Structures of Tall Building*, Beijing: China Ministry of Construction. (in Chinese)

Ji XD, Cheng XW and Xu MC (2018), "Coupled Axial Tension-shear Behavior of Reinforced Concrete Walls," *Engineering Structures*, **167**: 132–142.

Kassem W (2015), "Shear Strength of Squat Walls: a Strut-and-Tie Model and Closed-Form Design Formula," *Engineering Structures*, **84**: 430–438.

Kowalsky MJ and Priestley MJN (2000), "Improved Analytical Model for Shear Strength of Circular Reinforced Concrete Columns in Seismic Regions," *ACI Structural Journal*, **97**(3): 388–396.

Kwan AKH, Cheung YK and Lu XL (1994), "Large Scale Model Tests of Reinforced Concrete Slit Shear Walls," *International Journal of Structures*, **14**(2): 63–82.

Mau ST and Hsu TTC (1987), "Shear Behavior of Reinforced Concrete Framed Wall Panels with Vertical Loads," *ACI Structural Journal*, **84**(3): 228–234.

McLean DI and Smith CL (1997), *Noncontact Lap Splices in Bridge Column-Shaft Connections*, Pullman, Washington: Washington State University.

Peng Y, Wu H and Yan Z (2015), "Strength and Drift Capacity of Squat Recycled Concrete Shear Walls under Cyclic Loading," *Engineering Structures*, **100**: 356–368.

Peng YY, Qian JR and Wang YH (2010), "Cyclic Performance of Precast Concrete Shear Walls with a Mortar-sleeve Connection for Longitudinal Steel Bars," *Materials and Structures*, **49**(6): 2455–2469.

Qian JR, Zhang WJ, Zhao FD, Li LR, Meng T and Feng BC (2010), "Tests of Specimens of Double Piece Prefabricated Reinforced Concrete Hollow-Core Shear Wall," *Building Structure*, **40**(6): 71–75. (in Chinese)

Sagan VE, Gergely P and White RN (1988), *The Behavior and Design of Noncontact Lap Splices Subjected to Repeated Inelastic Tensile Loading*, Ithaca, NY: Cornell University.

Sánchez-Alejandre A (2009), "Comportamiento Sísmico de Muros de Concreto para Vivienda," *Ph.D. Dissertation*, Universidad Nacional Autónoma de México.

Sun ZJ, Liu JL and Chu MJ (2013), "Experimental Study on Behaviors of Adaptive-Slit Shear Walls," *The Open Civil Engineering Journal*, **7**: 189–195.

Wang ZJ, Liu WQ, Wei W and Ye YH (2012), "Experimental Study on Seismic Behavior of Reinforced Concrete Composite Shear Wall with Level Splice," *Journal of Building Structures*, **33**(7): 147–155. (in Chinese)

Xiao QD and Guo ZX (2014), "Experimental Study on Seismic Behavior of Double-wall Precast Concrete Shear Wall," *Advanced Materials Research*, **919**: 1812–1816.

Zhao ZZ, Zhou J, Hou JQ, and Ren BS (2015), "Review of Studies on Shear Resisting Mechanisms and Calculating Formulas of Shear Resisting Capacity of Horizontal Joints in Fabricated Reinforced Concrete Shear Wall Structures," *Building Structure*, **45**(12): 40–47. (in Chinese)

Zhou J, Zhao ZZ, Hou JQ, Ren BS, Chu MJ and Liu JL (2015), "Experimental Study on Seismic Behavior of Splice Rebar Connection Between Upper and Lower Floors of Shear Walls with Precast Concrete Hollow Moulds," *Journal of Building Structures*, **36**(6): 44–52. (in Chinese)